MRS Advances © 2019 Materials Research Society
DOI: 10.1557/adv.2019.56

A Multiscale Approach to Predict the Mechanical Properties of Copper Nanofoams

Hang Ke, Andres Garcia Jimenez, Ioannis Mastorakos

Department of Mechanical and Aeronautical Engineering, Clarkson University, Potsdam, NY 13699, US

ABSTRACT

Pure metallic nanofoams in the form of interconnected networks have shown strong potentials over the past few years in areas such as catalysts, batteries and plasmonics. However, they are often fragile and difficult to integrate in engineering applications. In order to better understand their deformation mechanisms, a multiscale approach is required to simulate the mechanical behavior of the nanofoams, although these materials will operate at the macroscale, they will still be maintaining an atomistic ordering. Hence, in this work we combine molecular dynamics (MD) and finite element analysis (FEA) to study the mechanical behavior of copper (Cu) nanofoams. Molecular dynamics simulations were performed to study the yield surface of a representative cell structure. The nanofoam structure has been generated by spinodal decomposition of binary alloy using an atomistic approach. Then, the information obtained from the molecular dynamics simulations in the form of yield function is transferred to the finite element model to study the macroscopic behavior of the Cu nanofoams. The simulated mechanical behavior of Cu nanofoams is in good agreement of the real experiment results.

INTRODUCTION

Metallic nanofoams made of materials such as copper (Cu), nickel (Ni), gold (Au) and platinum (Pt) have the potential to present clear advantages in a broad spectrum of low-density and high surface area applications. Their excellent surface to volume ratios make them great choice for catalysts [1], sensors [2], actuators [3], fuel cells [4] and plasmonics [5]. Despite such advantages, metallic nanofoams exhibit brittle behavior macroscopically due to plastic deformation in individual ligaments. In pure metallic nanofoams, the ligament strength does approach the theoretical strength, but there is almost no ability to strain harden, and hence local geometry fluctuations leads to premature macroscopic failure. This lack of macroscopic strength is one of the limiting factors in broadly applying metallic nanofoams. Overall, the mechanical behavior of a metallic

Downloaded from https://www.cambridge.org/core. Clarkson University, on 28 Jan 2019 at 16:33:49, subject to the Cambridge Core terms of use, available at https://www.cambridge.org/core/terms. https://doi.org/10.1557/adv.2019.56

nanofoam is determined by the relationship between the behavior of the ligaments of which this material is formed and the geometry of the ligaments.

For the past few years, large amounts of effort have been devoted to study the mechanical properties of metallic nanofoams. The Gibson and Ashby model [6] has been widely used for theoretical studies of nanofoams to estimate the yield strength, the elastic modulus and ultimate tensile strength. However, this model is not applicable for nano-scale porous foams because it fails to consider the microstructural parameters of ligaments, which consist the nanofoam. Hodge et al. [7] and Briot et al. [8] reported that the yield strength of metallic nanofoam varies with the ligament diameter and a modified scaling equation was proposed which incorporates the Hall-Petch relation. However, many reported models are focused either on microstructures which simulate those in real nanofoams or simplified geometrical models which neglects the atomistic configurations. In current work, we use a multiscale approach to predict the mechanical properties of Cu nanofoams with a random distribution of ligaments. MD simulations were performed to generate yield surfaces and FEA were performed to investigate the mechanical strength of the macroscopic Cu nanofoam.

METHODOLOGY

First, a randomly distributed foam structure was created. Previous works have used various techniques to generate the random foam structure. For example, Gunkelmann et al. [9,10] first built a template for the foam structure by starting with an fcc crystal with periodic boundary conditions. Then the crystal structure was heated above the melting temperature and atoms with temperature above a chosen value have been removed to get the desired porosity. Ngô et al. [11] and He et al. [12] generated the structure by a spinodal decomposition simulation of a binary mixture via Monte Carlo (MC) method. Crowson et al. [13,14] also model the spinodal decomposition of a binary alloy using a phase field method. Their sample presented similar shape to experimental observations in terms of ligament size distribution and surface curvature. In this work the method suggested by Gunkelmann [10] has been used. It has been reported that this technique results to similar foam macrostructures to that obtained using the analysis based on small-angle neutron scattering data considered for porous gold.

A simulation box consisting 40*40*40 Cu lattice spacing with (001) direction was formed. We randomly assign two types of atoms to the lattice sites: type 1 which represents Cu atom and type 2 which represents void. The relative density in our case here is 46%. After the spinodal decomposition process we remove the void part in the box and the final structure is shown using OVITO [15] in Figure 1. The simulation box has a side length of 14.4 nm, and the total number of Cu atoms is 138762.

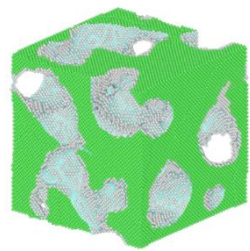

Figure 1. Atomistic configuration of Cu nanofoam cell structure.

Downloaded from https://www.cambridge.org/core. Clarkson University, on 28 Jan 2019 at 16:33:49, subject to the Cambridge Core terms of use, available at https://www.cambridge.org/core/terms. https://doi.org/10.1557/adv.2019.56

Then, MD simulations were performed using LAMMPS [16] with potentials based on the embedded atom method (EAM) [17,18]. The EAM potential used to describe the atomic interactions between Cu is given by Voter and Chen [19]. To model infinitely large nanofoams, periodic boundary conditions were applied along all three directions. In all simulations the temperature was kept constant at 300K during both the relaxation and loading steps. The isothermal-isobaric (NPT) ensemble was used to update the atomic velocities and positions at each step. The Cu nanofoam structure was subjected to uniaxial and hydrostatic and mixed compression stress states and the yield stress value has been recorded for each case. For the mixed loading, first the hydrostatic stress was reduced to a fraction (4/5, 3/5, 2/5 and 1/5) of the hydrostatic yield strengths, and a uniaxial compression was performed along z-direction until yield was achieved with the hydrostatic stress in the other two directions kept constant. The mean stress and the von Mises effective stress were calculated at the yield point of all simulation tests. Using this method, yield surfaces were generated and curve fitted into the isotropic constitutive model given by Deshpande [20]. The yield function Φ is defined by

$$\Phi \stackrel{\text{def}}{=} \hat{\sigma} - Y \leq 0. \tag{1}$$

And the equivalent stress $\hat{\sigma}$ is defined by

$$\hat{\sigma}^2 \stackrel{\text{def}}{=} \frac{1}{[1+(\alpha/3)^2]}[{\sigma_e}^2 + \alpha^2 {\sigma_m}^2]. \tag{2}$$

In this equation, σ_m is the mean stress $\sigma_m \stackrel{\text{def}}{=} \sigma_{kk}/3$, and σ_e is the von Mises effective stress $\sigma_e \stackrel{\text{def}}{=} \sqrt{\frac{3}{2}\sigma_{ij}'\sigma_{ij}'}$. We fit our results with this model and get the value of the parameter α, which defines the elliptical shape of the yield surface.

Then, this parameter α has been used in the FEA part to generate the macroscopic stress-strain curve of the copper nanofoam under compression. The original work by Deshpande used experimental data to find the hardening behavior of the theoretical model. However, very few of such data are available in the case of nanofoams. To account for that, the theoretical hardening model suggested by Hanssen et al. [21] has been used. This model has the advantage that also includes the foam density which is an important characterization parameter. Hanssen's hardening model is defined as

$$Y = Y_o + \gamma \frac{\hat{\varepsilon}}{\varepsilon_D} + \alpha_2 \ln\left(\frac{1}{1-(\hat{\varepsilon}/\varepsilon_D)^\beta}\right). \tag{3}$$

where Y_o is the yield strength, α_2, β, and γ are material parameters, and ε_D is the compaction strain $\varepsilon_D \stackrel{\text{def}}{=} 1 - \frac{\rho_f}{\rho_o}$. The material parameters α_2, β, and γ were obtained by fitting experimental results [22] of uniaxial compression testing on a Cu foam with elastic modulus of 1.7 GPa, yield strength of 12 MPa, and relative density of 40%. These material parameters depend on the foam relative density as defined by

$$\left\{\alpha_2, \gamma, \frac{1}{\beta}\right\} = C_0 + C_1\left(\frac{\rho_f}{\rho_o}\right)^n. \tag{4}$$

where C_0, C_1, and n are constants, which were determined by fitting the experimental data with Hanssen's hardening model. After obtaining the constants, the material parameters could be computed for different relative densities. FEA using MOOSE Framework [23] was performed for the metallic nanofoam generated in MD. For the elastic part of the Cu nanofoam, following the Hall Petch effect, the yield strength of the foam would vary depending on the ligament size; however, since the ligament diameters for the generated foam were random, the yield strength was considered to be the same as the experimental yield strength. The elastic modulus was determined using the scaling equation [6] described by $E = E_o(\rho_f/\rho_o)^2$, where E_o is the elastic modulus of bulk Cu. Finally, to evaluate the effects of density, different relative densities were considered for the

Downloaded from https://www.cambridge.org/core. Clarkson University, on 28 Jan 2019 at 16:33:49, subject to the Cambridge Core terms of use, available at https://www.cambridge.org/core/terms.
https://doi.org/10.1557/adv.2019.56

simulated nanofoam. Three cases were compared with relative density of 35%, 50% and 55% using the same α parameter obtained from MD simulations.

DISCUSSIONS

Molecular dynamics

The stress-strain curve for both uniaxial compression and hydrostatic compression are shown in Figure 2(a). The yield strengths of uniaxial compression and hydrostatic compression are 1.24 GPa and 1.35 GPa, respectively. The elastic modulus in the hydrostatic compression is significantly higher than in the uniaxial compression due to the anisotropic nature of the foam.

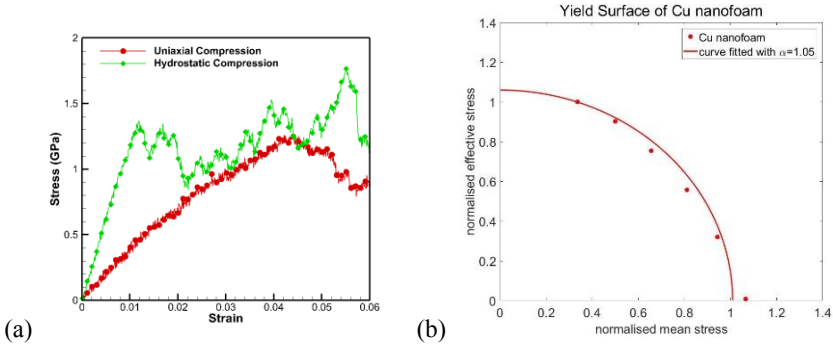

Figure 2. (a) The stress-strain curve for uniaxial and hydrostatic compression of the Cu nanofoam structure. (b) The yield surface of Cu nanofoam structure with curve fitting.

The yield surface of the Cu nanofoam cell structure is shown in Figure 2(b). The mean stress and effective stress are normalized with the uniaxial yield strength for comparison. The uniaxial point is the point with normalized effective stress is 1, and the hydrostatic point is the point with normalized effective stress is 0. All the six points are curve fitted into the yield equation with parameter $\alpha = 1.05$. This value is transferred to the FEA part for further calculations.

Finite element analysis

The curve fitting of the experimental data for the uniaxial compression using Hanssen's model is shown in Figure 3. Using the curve fitting, the constants describing the material parameters were determined and FEA was performed to confirm the accuracy of the fitting. Table 1 shows the numerical results of the curve fitting used in the FEA.

Table 1. Results of material parameters for FEA.

Factors	α_2 (MPa)	$1/\beta$	γ (MPa)
C_0	2.066	0.228	0.806
C_1	11.02	7.198	12.23
n	0.0135	1.614	0.0107

Downloaded from https://www.cambridge.org/core. Clarkson University, on 28 Jan 2019 at 16:33:49, subject to the Cambridge Core terms of use, available at https://www.cambridge.org/core/terms. https://doi.org/10.1557/adv.2019.56

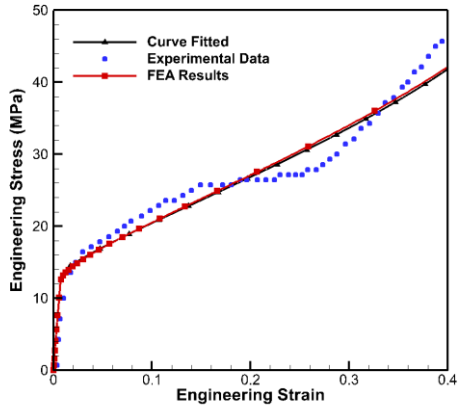

Figure 3. Curve fitting of experimental data using Hanssen's hardening model.

Once the accuracy of the fitting was confirmed, the material parameters were calculated for each relative density of the MD generated foam as shown in Table 2.

Table 2. Material parameters used in FEA simulations.

Foam	ρ_f/ρ_o	ε_D	E (GPa)	Y_o (MPa)	α_2 (MPa)	$1/\beta$	γ (MPa)
Experimental	0.40	0.60	1.70	12	12.95	1.87	12.92
1	0.46	0.54	26.1	12	12.97	2.28	12.93
2	0.50	0.50	31.0	12	12.98	2.58	12.95
3	0.35	0.65	15.2	12	12.93	1.55	12.90
4	0.55	0.45	37.5	12	12.99	2.97	12.96

Using the material parameters from Table 2, FEA was performed for each relative density and the results were compared to the experimental data as depicted in Figure 4. The variance in the elastic region is caused by the differences in elastic moduli. Comparing the FEA results of the MD generated foam shows that denser foams are stronger as they contain more material helping them withstand higher compressive stresses.

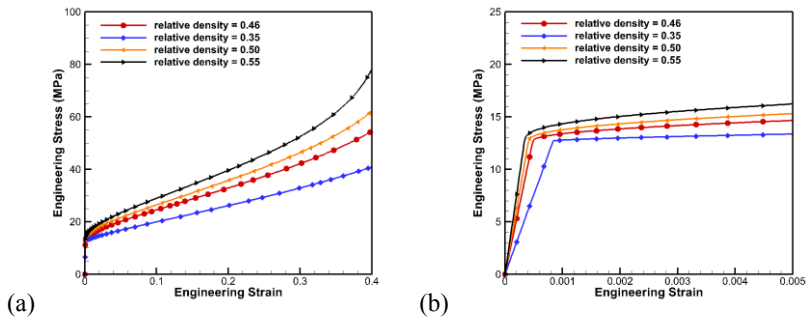

Figure 4. FEA results for the Cu nanofoams with different densities. (a) plastic region, (b) elastic region.

Downloaded from https://www.cambridge.org/core. Clarkson University, on 28 Jan 2019 at 16:33:49, subject to the Cambridge Core terms of use, available at https://www.cambridge.org/core/terms. https://doi.org/10.1557/adv.2019.56

CONCLUSIONS

A multiscale approach to predict the mechanical properties of Cu nanofoams is presented in our work. First, the nanoporous foam structure has been constructed through spinodal decomposition method using atomistic simulations. Then, the yield surface of this structure was generated using molecular dynamics and the results were curve fitted with a yield equation with the mean stress and effective stress. Finally, finite element analysis has been performed to simulate the mechanical behavior of Cu nanofoams under uniaxial compression test. The simulated results were shown to be in good agreement with experiment findings. The application of this method can be used to predict the mechanical behavior of macroscopic nanofoam specimens under complex loading conditions, maintaining an atomistic order resolution.

ACKNOWLEDGMENTS

The authors would like to thank Dr. David Bahr from Purdue University for his useful discussions. This research work was sponsored by the National Science Foundation (NSF) under collaborative Grants Nos. CMMI 1634640 and CMMI 1634772.

REFERENCES

[1] A. Wittstock, V. Zielasek, J. Biener, C. M. Friend, and M. Bäumer, Science **327**, 319 (2010).
[2] L. Y. Chen, T. Fujita, and M. W. Chen, Electrochimica Acta **67**, 1 (2012).
[3] J. Biener, A. Wittstock, L. A. Zepeda-Ruiz, M. M. Biener, V. Zielasek, D. Kramer, R. N. Viswanath, J. Weissmüller, M. Bäumer, and A. V. Hamza, Nat. Mater. **8**, 47 (2009).
[4] E. Antolini, Energy Environ. Sci. **2**, 915 (2009).
[5] J. Biener, G. W. Nyce, A. M. Hodge, M. M. Biener, A. V. Hamza, and S. A. Maier, Adv. Mater. **20**, 1211 (2008).
[6] L. J. Gibson and M. F. Ashby, *Cellular Solids: Structure and Properties* (Cambridge University Press, 1997). p. 186.
[7] A. M. Hodge, J. Biener, J. R. Hayes, P. M. Bythrow, C. A. Volkert, and A. V. Hamza, Acta Mater. **55**, 1343 (2007).
[8] N. J. Briot and T. J. Balk, Philos. Mag. **95**, 2955 (2015).
[9] N. Gunkelmann, Y. Rosandi, C. J. Ruestes, E. M. Bringa, and H. M. Urbassek, Comput. Mater. Sci. **119**, 27 (2016).
[10] N. Gunkelmann, E. M. Bringa, and Y. Rosandi, J. Phys. Chem. C **122**, 26243 (2018).
[11] B.-N. D. Ngô, A. Stukowski, N. Mameka, J. Markmann, K. Albe, and J. Weissmüller, Acta Mater. **93**, 144 (2015).
[12] L. He and N. Abdolrahim, Comput. Mater. Sci. **150**, 397 (2018).
[13] D. A. Crowson, D. Farkas, and S. G. Corcoran, Scr. Mater. **61**, 497 (2009).
[14] D. A. Crowson, D. Farkas, and S. G. Corcoran, Scr. Mater. **56**, 919 (2007).
[15] A. Stukowski, Model. Simul. Mater. Sci. Eng. **18**, 015012 (2010).
[16] S. Plimpton, J. Comput. Phys. **117**, 1 (1995).
[17] M. S. Daw and M. I. Baskes, Phys. Rev. B **29**, 6443 (1984).
[18] M. S. Daw, S. M. Foiles, and M. I. Baskes, Mater. Sci. Rep. **9**, 251 (1993).
[19] A. F. Voter and S. P. Chen, MRS Online Proc. Libr. Arch. **82**, (1986).
[20] V. S. Deshpande and N. A. Fleck, J. Mech. Phys. Solids **48**, 1253 (2000).
[21] A. G. Hanssen, O. S. Hopperstad, M. Langseth, and H. Ilstad, Int. J. Mech. Sci. **44**, 359 (2002).
[22] J. Gubicza, P. Jenei, K. Nam, C. Kádár, H. Jo, and H. Choe, Mater. Sci. Eng. A **725**, 160 (2018).
[23] D. R. Gaston, C. J. Permann, J. W. Peterson, A. E. Slaughter, D. Andrš, Y. Wang, M. P. Short, D. M. Perez, M. R. Tonks, J. Ortensi, L. Zou, and R. C. Martineau, Ann. Nucl. Energy **84**, 45 (2015).

Downloaded from https://www.cambridge.org/core. Clarkson University, on 28 Jan 2019 at 16:33:49, subject to the Cambridge Core terms of use, available at https://www.cambridge.org/core/terms. https://doi.org/10.1557/adv.2019.56